Degradable 4D-printed hydration-driven actuators from a single family of amphiphilic star-shaped copolymers

Grosjean, Mathilde; Schmidleithner, Christina; Dejean, Stéphane; Larsen, Niels B.; Nottelet, Benjamin

Published in:
Materials and Design

Link to article, DOI:
10.1016/j.matdes.2024.112953

Publication date:
2024

Document Version
Publisher's PDF, also known as Version of record

Materials & Design 241 (2024) 112953

Contents lists available at ScienceDirect

Materials & Design

journal homepage: www.elsevier.com/locate/matdes

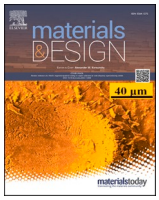

Degradable 4D-printed hydration-driven actuators from a single family of amphiphilic star-shaped copolymers

Mathilde Grosjean [a], Christina Schmidleithner [c], Stéphane Dejean [a], Niels B. Larsen [c,*], Benjamin Nottelet [a,b,*]

[a] Polymers for Health and Biomaterials, IBMM, Univ Montpellier, CNRS, ENSCM, 34090 Montpellier, France
[b] Department of Pharmacy, Nîmes University Hospital, Univ Montpellier, 30900 Nimes, France
[c] Department of Health Technology, DTU Health Tech, Technical University of Denmark, 2800 Kgs. Lyngby, Denmark

ARTICLE INFO

Keywords:
Actuator
Stereolithography
4D printing
star PEG-PLA copolymer
Dual material printing
Numerical modeling

ABSTRACT

Actuators are largely used in biomedical applications in the presence of sensitive live cells or biomolecules, which makes actuators triggered by water uptake highly appealing. Dual-material printing and hydration driven expansion is a method of choice to produce such actuators, but mostly rely of non-degradable polymers or on the combination of polymers of different nature that may lead to interface incompatibilities. To overcome this challenge, we report here on two photocrosslinkable resins based on a single family of degradable hydrophilic or hydrophobic star-shaped poly(ethylene glycol)-poly(lactide) copolymers. The two materials are first printed individually and characterized to ensure that their properties enable the printing of dual material objects by stereolithographic digital-light processing. Dual-materials actuators are then printed by sequential switching of the hydrophobic and hydrophilic resin baths. Objects of simple and complex shapes are easily obtained and exhibit rapid actuation (<60 s) upon hydration. The swelling-induced shape changes are accurately reproduced by numerical modeling of the printed geometries using the obtained material swelling properties. This set of results offers new perspectives to develop 4D-printed temporary medical devices.

1. Introduction

Polymeric actuators rely on materials able to change their shape in response to a stimulus. They are of great interest for the development of smart materials and devices and have therefore appeared in a broad range of fields in the recent years, including biomedical applications [1,2]. The use of polymers enables both the design of hard actuators, as well as soft actuators compatible with soft living tissues and present the advantages to be easily processed in a wide range of forms and shapes [3,4]. Moreover, many polymers are biocompatible and biodegradable, which allows the integration of actuators in living systems followed by their resorption. Finally, polymers can be sensitive to different stimuli, which enables the development of actuators controlled by temperature, pH, biological signals, light, or solvent absorption [5].

Based on the mechanism involved, polymeric actuators can be classified into four categories [1,2]. The first group gathers the systems based on elastic relaxation of shape after deformation and mainly includes shape memory polymers [6]. In these systems, the permanent shape is determined by the crosslinking. When the polymer is heated, it becomes flexible and can be easily deformed. The deformed shape can then be frozen by cooling the material below the melting temperature or glass-transition point, where the mobility of the chains of the polymer is limited. Finally, the initial shape can be restored by increasing the polymer chain mobility when the temperature is increased. The second category is liquid-crystalline actuators, which are hierarchical materials that display a defined microstructure over macroscopic length scales and can stretch or shrink anisotropically along the director orientation when the order parameter is affected, for instance by a change in temperature or chemical environment [7]. The third family is composed of actuators based on a reversible change in the volume, including hydrogels that can swell and shrink in aqueous environment or humid air [8], or materials able to change in volume due to thermal expansion and shrinking or melting and crystallization [9,10]. Finally, the fourth category focuses on actuators for which the driving force is surface tension. Their development is strongly dependent on the size of the systems. Indeed, at a macroscale the contribution of surface tension is negligible, and the

* Corresponding authors at: Polymers for Health and Biomaterials, IBMM, Univ Montpellier, CNRS, ENSCM, 34090 Montpellier, France (B. Nottelet).
E-mail addresses: nibl@dtu.dk (N.B. Larsen), benjamin.nottelet@umontpellier.fr (B. Nottelet).

https://doi.org/10.1016/j.matdes.2024.112953
Received 6 February 2024; Received in revised form 13 April 2024; Accepted 16 April 2024
Available online 17 April 2024

movement is produced due to a change in the internal properties of the polymers. When the size of the actuators is diminished to the microscale or nanoscale, the role of surface tension becomes significant and can enable the design of actuators driven by surface tension. Of notice, besides research on biomaterials and their combination, optimization of actuation, of its predictability and of its autonomous character are currently investigated in the frame of soft robots by addition of topology optimization approaches, finite element methods and machine learning [11,12].

Actuators have been developed for various biomedical applications [13,14], including soft robotics [15–19], tissue engineering [20], delivery systems [21–28], and organ-on-chip [29–31]. Within this fields, the possibility to 3D-print actuators to yield high resolution 4D printed devices/scaffolds as recently emerged as a prime opportunity. However, although 4D printing is gaining in popularity, recent reviews clearly points out major challenges [32–34]. First, 4D printing is often restricted to non-degradable materials as the number of fully degradable polymers suitable for high resolution printing remains low. Second, most 4D printed biomaterials rely on thermal triggers with temperatures out of the physiological range, making them incompatible with tissues. Therefore, to be used in the presence of sensitive cells or active molecules, developing systems in which the motion is driven by hydration becomes of great interest. Third, the opposition between the printing of high mechanical properties objects (which require high molar masses) and high-resolution printability (which requires low viscosities) remains prevalent and is generally solved by using reactive dilutants [35,36] that put to risk the degradability and compatibility of the resulting biomaterials. Finally, the printing of high resolution multi-material actuators is still limited as stereolithography is usually limited to the printing of one material at a time [37–39]. Some methods have been proposed to overcome this limitation but are all associated with drawbacks. The first and simplest method consists in preparing several resins and switching the bath during printing [40,41]. This method is often associated with delamination problems as immersing the printed part in the second resin may induce uncontrolled swelling or shrinking which compromises the adhesion of the second material to the first one. Another method is based on the use of a single resin and tuning the properties of the materials within the bulk by varying the crosslinking (*e.g.*, grayscale illumination [42–44]) or post-curing conditions [45]. In the last technique, a single resin containing several macromers is used. By playing on the functional groups of the macromers and depending on the wavelength and initiators used, a crosslinking reaction can be initiated preferentially to another [46–48].

Taking these challenges and constraints into account only few combinations of materials have been reported so far to yield degradable hydration-driven 4D-printed actuation systems. The combination of biopolymers (gelatin, hyaluronic acid, alginate) is an example, but is limited to very soft actuators due to the hydrogel nature of the resulting constructs that are restricted to bioinks and tissue engineering applications. For scaffolds or medical devices requiring higher mechanical properties, synthetic materials are preferred. Degradable poly(ester urethane) or polyesters have been combined with hyaluronic acid hydrogels or acrylic-based hydrogels to yield at least partly degradable actuators [49,50]. However, the different nature of the components used may put a threat on an optimal transfer of stress. To the best of our knowledge, the only tentative to produce 3D printed hydration-based actuators using a single type of polymers has been reported by Song *et al.* who used two non-degradable polyurethane elastomers [51].These examples clearly point out the lack of materials that have been designed to combine degradability, distinct swellability, compatibility with printing processes and a similar chemical nature.

In response to these challenges, we propose the DLP-based stereolithography printing of a single family of degradable star-shaped poly (ethylene glycol)-poly(lactic acid) (PEG-PLA) photopolymers recently developed by our group to prepare 4D printed water-swelling responsive actuators. The rational for this choice of copolymers relies on their star topology enabling the formulation of resins with suitable viscosity despite high molecular weight polymers, and the possibility to soundly select (compositions and molecular weight) and associate (elastomer/hydrogel bilayer) such copolymers to generate spontaneous and rapid actuation when immersed in water [52]. In more details, a hydrophobic $PEG_{8arm}10k\text{-}(PLA_{69})_8$-methacrylate (MC) and a hydrophilic $PEG_{8arm}20k\text{-}(PLA_{13})_8$-MC are formulated in distinct photoresins. The cure depth as a function of the irradiation time is first studied to determine the 3D-printing conditions. The two materials are printed separately and characterized through gel fraction, volume shrinkage, water uptake and volumetric swelling measurements to ensure that the properties of each independent material allow for the preparation of dual material constructs. Dual materials constructs are then printed based on the manual resin bath switching method. Similar shrinkage and cohesion of the two layers are ensured by the similar chemical structure of the two copolymers, which enables the use of resins of similar compositions. Objects of simple structures but also more complex shapes are obtained. Finally, actuation of a complex 3D printed designs according to their 3D structure are demonstrated upon immersion in water. Numerical modeling of the swelling process is shown to accurately predict the geometry of the final swollen state of the dual-material actuators, which in future applications could be employed to predict the required 3D printed geometry to achieve a targeted actuator motion pattern.

2. Materials and methods

2.1. Materials

$PEG_{8arm}10k\text{-}(PLA_{69})_8$-MC and $PEG_{8arm}20k\text{-}(PLA_{13})_8$-MC were synthesized and characterized as described in our previous study [52]. In addition, Irgacure 819, Sudan I, and propylene carbonate were purchased from Sigma-Aldrich.

2.2. Resin formulation

After optimization, the following resin composition was used: $PEG_{8arm}10k\text{-}(PLA_{69})_8$-MC or $PEG_{8arm}20k\text{-}(PLA_{13})_8$-MC (300 $mg.mL^{-1}$), Irgacure 819 (10 $mg.mL^{-1}$), Sudan I (1 $mg.mL^{-1}$) and propylene carbonate (solvent). The different components were solubilized in the solvent until a homogeneous resin was obtained. When needed, an ultrasonic bath was used. The bath temperature was controlled to avoid unintentional crosslinking.

2.3. Determination of cure depth

50 μL of resin was deposited on a glass coverslip, which was placed in the transparent printer vat. The sample was flood-irradiated for a specific time at a wavelength of 365 nm. The excess of uncured resin was removed with paper tissue and the thickness of the cured part was measured with a micrometer. The measurements were performed for both polymers for exposure times ranging from 5 to 30 s.

2.4. 3D printing conditions

The 3D printing was performed using a custom-built stereolithography printer and methacrylate-silane treated cover-glasses were used as build-supports to ensure adhesion of the printed part [46,53].

Autodesk Inventor Professional 2022 (Autodesk) was used to generate 3D designs exported as STL files, and the open-source Slic3r software was employed for slicing into exposure images for the individual print layers.

For each print, at least 1.5 mL of the resin solution was added to the printer vat, having a transparent bottom for light exposure from below. Each 20 μm thick layer was illuminated at 365 nm for 7 s at a power density of 12 mW/cm^2. To ensure good adhesion to the cover-glass, the first four layers were printed with a nominal thickness of 5 μm and the

next two with a nominal thickness of 10 μm, each exposed for 10 s. After printing, the objects were washed in acetone for 24 h with solvent-changes three times a day. Then, the samples were dried under vacuum.

2.5. Gel fraction

Cylinders of 5 mm diameter and 5 mm height (volume of 98.1 mm^3 = 0.098 mL) were printed. Then, the samples were washed in acetone for 24 h with solvent-changes three times a day before being dried under vacuum and weighed.

As the initial polymer concentration in the resin is 300 $mg.mL^{-1}$, the final expected mass of polymer in a cylinder is 29.4 mg.

The gel fraction was determined by comparing the final experimental mass of a cylinder with the theoretical mass according to equation (1). The experiment was run with n = 6.

$$\text{Gel fraction} = \frac{\text{Experimental mass}}{\text{Theoretical mass}(29.4\text{mg})} \quad (1)$$

2.6. Volume shrinkage

Cylinders of 5 mm diameter and 5 mm height (volume V_{print} of 98.1 mm^3 = 0.098 mL) were printed. Then, the samples were washed in acetone for 24 h with solvent-changes three times a day before being dried under vacuum. Finally, the diameter and height of the cylinders were measured with a micrometer and used to calculate the final volume of the samples.

The volume shrinkage was determined by comparing the final volume of a cylinder after washing and drying with the initial volume of a cylinder just after printing according to equation (2). The experiment was run with n = 6.

$$\text{Volume shrinkage} = 1 - \frac{V_{final}}{V_{print}(98.1\text{mm}^3)} \quad (2)$$

2.7. Water uptake, volumetric swelling and actuation

Cylinders of 5 mm diameter and 5 mm height (volume of 98.1 mm^3 = 0.098 mL) were printed. Then, the samples were washed in acetone for 24 h with solvent-changes three times a day before being dried under vacuum.

Samples were weighed (W_i = initial weight), measured (V_i = initial volume) and placed in 5 mL of water at room temperature under stirring. At different time points, samples were removed from water, weighed (W_x = weight of the wet samples after x time in water) and measured (V_x = volume of the wet samples after x time in water). The water uptake and the volumetric swelling of the samples were calculated from equation (3) and (4). The experiment was run with n = 6.

$$\text{Water uptake} = \frac{W_x - W_i}{W_i} \quad (3)$$

$$\text{Volumetric swelling} = \frac{V_x - V_i}{V_i} \quad (4)$$

For actuation experiments, the printed dual-material objects were immersed in water at room temperature.

2.8. Numerical modeling

COMSOL Multiphysics 6.1 (COMSOL) was employed to numerically model the time-dependent swelling of dual-material printed objects using Finite Element Modeling. The initial non-swollen model geometry was designed to match the dimensions of the washed and dried printed object geometry to account for the removal of the resin solvent fraction and uncured resin components after printing, i.e., a reduction in linear dimensions to 62 % of the design in all three dimensions to match the volumetric shrinkage to $(0.62)^3 = 0.24$ (76 % volumetric shrinkage, Table 1) of the printed volume on washing and drying. Water uptake was modeled by diffusion from a pure water phase at all outer object boundaries with a diffusion constant $D = 8{\cdot}10^{-10}m^2/s$ for both material types, optimized to match the experimentally observed rate of swelling for printed objects of each material. Swelling coefficients of $\beta_{hydrophilic} = 4.8{\cdot}10^{-4}m^3{\cdot}kg^{-1}$ and $\beta_{hydrophobic} = 1.1{\cdot}10^{-4}m^3{\cdot}kg^{-1}$ for the $PEG_{8arm}20k$-$(PLA_{13})_8$-MC and the $PEG_{8arm}10k$-$(PLA_{69})_8$-MC materials, respectively, were calculated from measurements of water uptake and volumetric swelling of the two materials printed separately.

Table 1
Properties of the materials based on $PEG_{8arm}10k$-$(PLA_{69})_8$-MC and $PEG_{8arm}20k$-$(PLA_{13})_8$-MC processed by stereolithography 3D printing. Data are expressed as the mean ± SD and correspond to measurements with n = 6.

Copolymer	Gel fraction (%)	Shrinkage (%)	Water uptake (%)	Volumetric swelling (%)
$PEG_{8arm}10k$-$(PLA_{69})_8$-MC	92.3 ± 2.6	76.0 ± 1.0	21.1 ± 0.9	37.0 ± 4.9
$PEG_{8arm}20k$-$(PLA_{13})_8$-MC	94.8 ± 2.9	75.8 ± 1.6	176.5 ± 1.3	226.2 ± 7.9

Both printed materials were modeled as being linear elastic and having a Poisson's ratio of 0.45. Prior reports have in detailed considered the modeling of water-induced swelling of nonlinear elastic materials with a fundamental outset in contributions to free energy change of the hydrogel during swelling [54,55]. The more accurate predictions of such models come with a requirement for providing detailed material characteristics beyond standard mechanical testing. The linear elastic approximation in our model is supported by the nearly linear stress–strain relation of the individual cross-linked materials for strains up to 80 % [52]. Elastic moduli of $E_{hydrophilic} = 3.1\,MPa$ and $E_{hydrophobic} = 2.4\,MPa$ were obtained in our previous report [52]. Objects were modeled with 4-way vertical axial symmetry for cylinders, i.e., using arc segments, or with a center line vertical symmetry plane perpendicular to the extruded hydrophilic bars of the actuator objects. The two material domains were separately meshed using a free triangular end-face mesh having a maximum element size of 70 μm swept equidistantly along the extrusion axis with an element width of 200 μm. In the actuator modeling, a mechanical fixed constraint was applied on a 50 x 50 μm square at the bottom center of the hydrophobic part. Numerical modeling proceeded by temporal tracking of water diffusion into each object ("Transport of Diluted Species" module) followed by modeling of the internal mechanical stress field and resulting object deformation ("Solid Mechanics" module) for each time point. The deformed objects are presented as either mirrored (actuators) or two-fold mirrored (cylinders) representations of the computed volumes for easier visual comparison to the 3D printed objects.

3. Results and discussion

3.1. Adjustment of the printing conditions

The initial step of this work was to determine the printing conditions of the materials. As the printer operated at a wavelength of 365 nm, the composition of the resins was optimized according to this parameter. The main component of a resin for stereolithographic 3D printing is the macromer, which must be photocrosslinkable since stereolithography produces 3D objects by light-induced resin solidification, most commonly by radical photopolymerization. In this case, two resins based on hydrophobic $PEG_{8arm}10k$-$(PLA_{69})_8$-MC or hydrophilic $PEG_{8arm}20k$-$(PLA_{13})_8$-MC were prepared. These polymers were selected because their combination demonstrated the best results regarding the design of self-rolling tubes in a previous study reported by our group [52]. Thanks to the presence of photoreactive methacrylate moieties at the chain-ends,

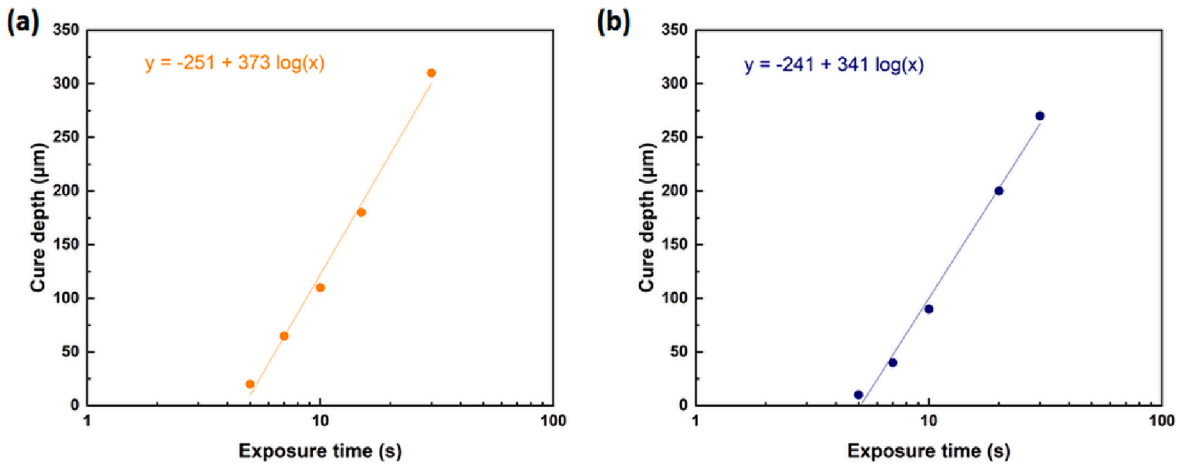

Fig. 1. Working curves at 365 nm for the resin based on (a) PEG_{8arm}10k-$(PLA_{69})_8$-MC and (b) PEG_{8arm}20k-$(PLA_{13})_8$-MC, showing cure depth as a function of exposure time with regression curves.

these copolymers are suitable for radical photopolymerization. For either polymer, the concentration was set at 300 mg.mL^{-1}. This value appeared as the best compromise to obtain a low-viscosity resin that allows for easy printing and 3D objects capable of maintaining their structure after curing. Propylene carbonate was chosen as solvent because it is non-toxic and is compatible with the various components of the 3D printer. Its role is to solubilize the constituents to obtain a homogeneous resin. A resin for stereolithography 3D printing also includes a photoinitiator and an absorber. Their quantities must be adjusted to reach the best compromise between printing speed and good resolution. As demonstrated in our previous study, the methacrylate functional star-shaped copolymers were able to achieve high crosslinking efficiencies without the use of photoinitiators [52]. Here, in order to minimize the time required for printing, Irgacure 819 was added to the resin composition at a concentration of 10 mg mL^{-1}. Indeed, an important factor for successful printing is fast light-induced solidification. Each layer is cured successively, so the exposure time needed for sufficient conversion at the appropriate wavelength must be minimized to reduce the printing time. The use of Irgacure 819 allows to initiate the radical polymerization when exposed at 365 nm, thus generating the crosslinked network. Finally, the absorber is used to control the layer cure depth while still allowing for sufficient layer-to-layer adhesion. Indeed, to obtain a 3D construct of good resolution, the crosslinking should be limited to the sliced layer. However, for the object to be built, there must be a slight interpenetration between neighboring layers. Sudan I was selected as the absorber and a concentration of 1 mg.mL^{-1} was used, based on prior results from our group [46].

To determine the thickness of the layers and the exposure time, a study of the crosslinking depth as a function of time was carried out. Working curves according to Jacobs [56] were created for the two resins (Fig. 1). According to equation (5), there is a relationship between the cure depth and the energy provided by the light irradiation, related to the exposure time.

$$C_d = D_p \log\left(\frac{E_{max}}{E_c}\right) = D_p \log E_{max} - D_p \log E_c \quad (5)$$

C_d refers to cure depth, D_p is the penetration depth of light, E_{max} is the dose of the incident light, and E_c is the critical energy necessary for polymerization.

At an exposure time of 7 s, both systems exhibited a cure depth above 20 µm with 65 and 40 µm for PEG_{8arm}10k-$(PLA_{69})_8$-MC and PEG_{8arm}20k-$(PLA_{13})_8$-MC, respectively. These results supported the selection of a printing time of 7 s per 20 µm layer. The larger cure depth will allow layer-to-layer adhesion and thus ensure robust printing.

3.2. 3D-printing of single materials and characterization

Once the printing conditions were set up, the two materials were printed separately and characterized via gel fraction, shrinkage, water uptake, and volumetric swelling measurements. These analyses were performed to ensure that the properties of each independent material

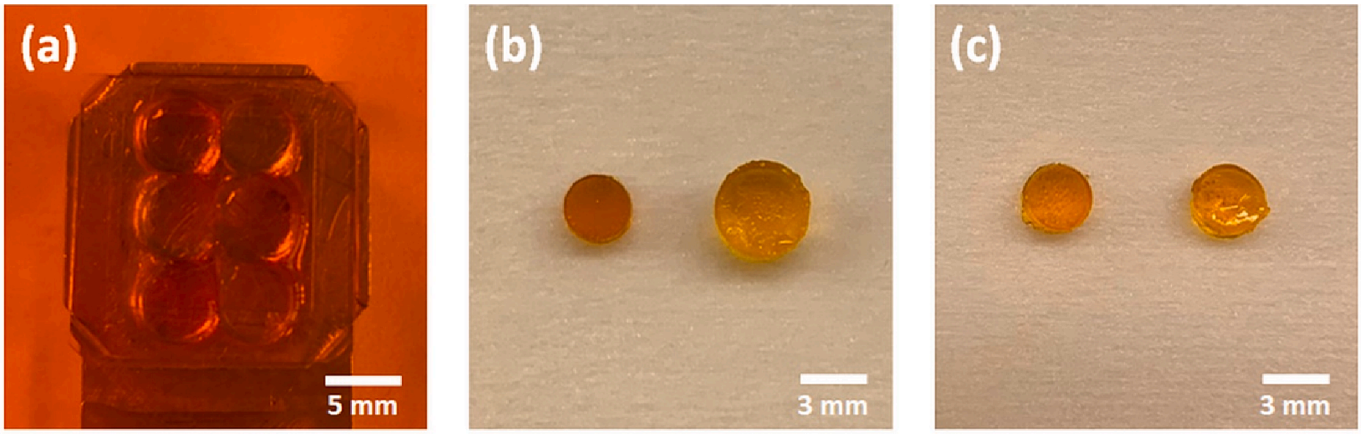

Fig. 2. Pictures of 3D-printed single materials: (a) example of cylinders just after printing, cylinders based on (b) PEG_{8arm}20k-$(PLA_{13})_8$-MC and (c) PEG_{8arm}10k-$(PLA_{69})_8$-MC after washing and drying (left) and after swelling in water (right).

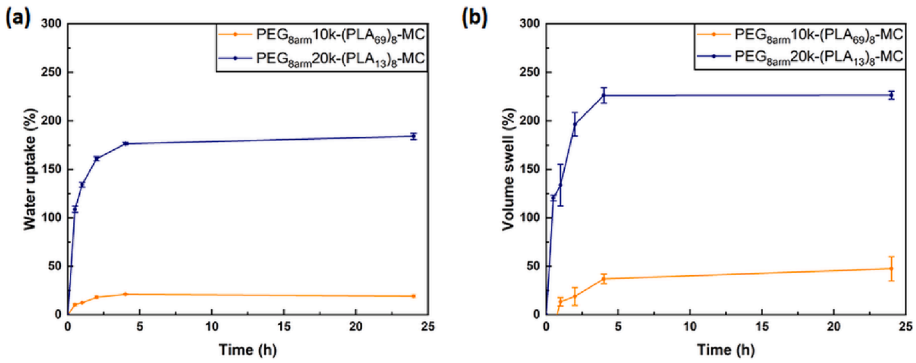

Fig. 3. Water uptake of the networks: (a) mass, (b) volume. Data are expressed as the mean ± SD and correspond to measurements with n = 6.

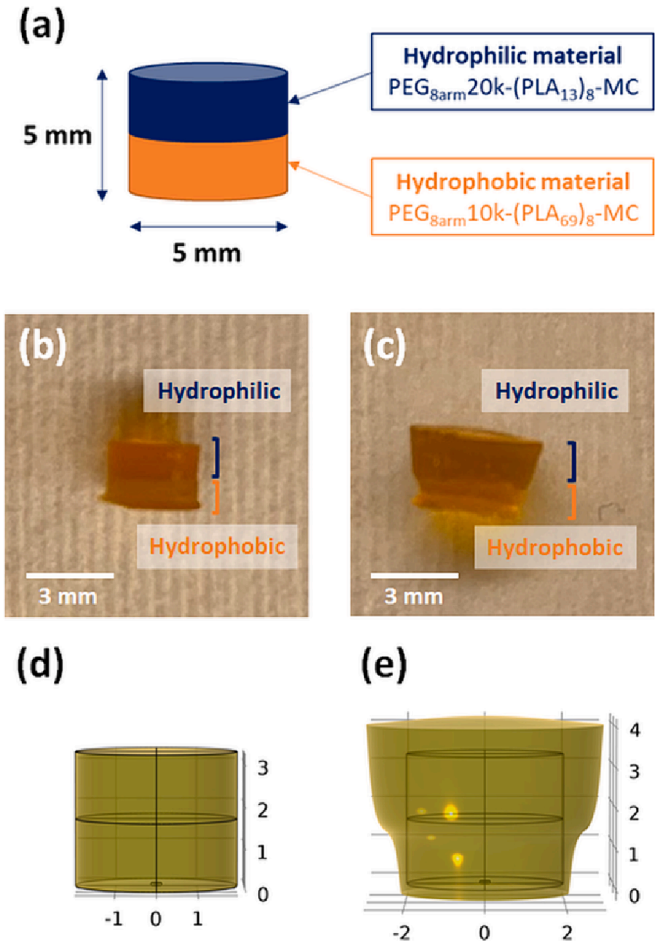

Fig. 4. (a) Schematic representation of dual material cylinder. Photos in side view of the 3D printed dual material cylinder (b) after post-treatment and (c) after immersion in water. Perspective renditions of the numerically modeled swelling process (d) before exposure to water and (e) after reaching steady-state swelling.

would allow for the printing of dual material objects. The results are presented in Table 1.

For each material, cylinders of 5 mm diameter and 5 mm height were printed (Fig. 2). The samples were then washed in acetone and dried under vacuum to obtain the final objects.

First, gel fraction measurements were carried out to quantify the photopolymerization efficiency. The final theoretical mass of polymer in a cylinder on complete curing was calculated to be 29.4 mg based the initial concentration of polymer in the resin and the volume of the cylinder just after printing. Comparison to the experimentally measured masses of the cylinders after post-treatment showed that both printed materials exhibited gel fractions above 90 %, with 92.3 % and 94.8 % for $PEG_{8arm}10k\text{-}(PLA_{69})_8$-MC and $PEG_{8arm}20k\text{-}(PLA_{13})_8$-MC, respectively. These results confirmed the efficient formation of crosslinked networks. The lower gel fraction of $PEG_{8arm}10k\text{-}(PLA_{69})_8$-MC can be explained by its higher molecular weight (50 000 vs. 27 500 $g.mol^{-1}$).

Finally, as the objective was to prepare materials with actuation properties based on the differences of swelling when immersed in water, the water uptake and the volumetric swelling of the two materials were studied for 24 h (Fig. 3). At different time points, the weight and the volume of the samples were compared to their initial weight and volume, after printing and post-treatment. The water uptake and the volume of the cylinders increased with time to reach a plateau after 4 h. As expected, the material based on hydrophilic $PEG_{8arm}20k\text{-}(PLA_{13})_8$-MC (EG/LA = 4.4) displayed higher absorption capacities with a water uptake of 176 % and a volumetric swelling of 226 % against only 21 % and 37 % for hydrophobic $PEG_{8arm}10k\text{-}(PLA_{69})_8$-MC (EG/LA = 0.4). These differences in terms of swelling should make it possible to develop systems able to actuate by immersion in water as demonstrated in our recent work [52].

3.3. 3D printing of dual material objects

Both polymers were able to be processed by stereolithographic 3D printing, and their properties appeared to be compatible with the design of a dual material object. Thus, the next step consisted in combining the two materials into one single object of simple shape to establish suitable printing conditions for a stable interface between the materials. Therefore, cylinders in which the two materials were superimposed, as described on the scheme in Fig. 4a, were printed. For this purpose, the hydrophobic part was first processed. When the printing was finished, the excess of hydrophobic resin was removed and replaced by the hydrophilic resin. A new print was then started with the height of the hydrophobic part as starting point. The main challenge was to make the second material adhere to the first one. This difficulty was easily overcome by the use of polymer of the same nature, as well as resins with similar compositions. The fact that the same solvent could be used for both polymers avoided shrinkage problems that could have occurred if the solvent had been changed between the two steps. In case of shrinkage, the required start height for the printing of the second part would change with time. Thus, dual material cylinders were printed successfully, and no delamination occurred during the post-treatment thanks to the similar shrinkage of the two materials during washing and drying steps (Fig. 4b). As expected, immersing the printed object in water resulting in a change to its shape, from a cylinder to a goblet-like geometry. As shown on Fig. 4c, the hydrophilic part swelled unlike the hydrophobic part that kept its original dimensions. The resulting dimensional mismatch at the interface of the materials induced local compressive strain of the hydrophilic material and local tensile strain of

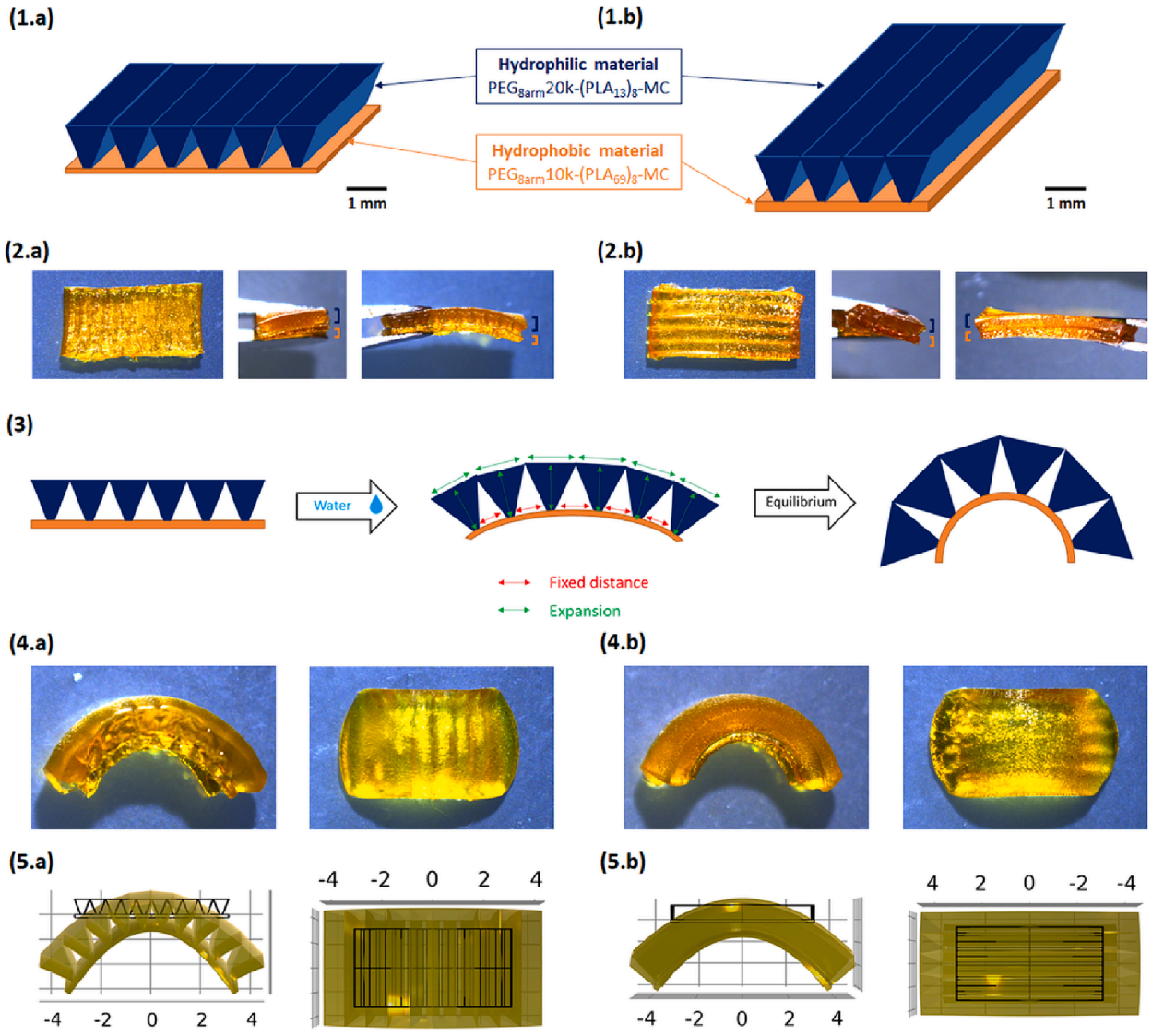

Fig. 5. (1) Schematic representation of the designed structures of the dual materials with the pyramid-shaped lines oriented (a) widthwise or (b) lengthwise. (2) Photos of the 3D printed constructs after post-treatment seen from the structured side (left) and in sideview (center and right). (3) Schematic representation of the expected change of shape. (4) Photos of the 3D printed constructs after swelling in water. (5) Numerical modeling of the 3D printed post-processed geometries after swelling in water.

the hydrophobic material. Again, no delamination occurred at this stage because of the strong adhesion at the interface between the two materials. Thus, this experiment confirmed the possibility to develop 3D-printed actuators able to change their shape thanks to the swelling differences between the materials.

Numerical modeling of the water absorption process and resulting swelling of the 3D printed post-treated dual material cylinder (Fig. 4b) accurately replicated the final swollen 3D geometry (Fig. 4d). The temporal shape changes during swelling (Supporting Information, Movie M1) were also well reproduced by the numerical model, as assessed by visual inspection of the printed cylinders upon immersion in water.

Finally, the work focused on the preparation of more complex actuating structures. Guided by their 3D design, the constructs should be able to curl into a controllable 3D shape upon immersion in water. The idea was to develop a construct for which the change of shape was mainly guided by the swelling of the hydrophilic part. The designed structure was composed of a flat hydrophobic layer on which is added the hydrophilic part that consists of connected bars of linearly extruded triangles. The triangular design of the array of extruded highly swellable hydrophilic material was chosen to support a hinged rotation between neighboring extruded volumes and to enable less residual stress at the interface between the materials at the equilibrium degree of swelling than if designing for full interfacial contact between the two materials having very different degrees of swelling. In order to experimentally assess the role of the hydrophilic layer on the direction of the shape change, two structures were designed with the array of hydrophilic bars being parallel to the shorter or longer dimension of the hydrophobic rectangular base, as shown on Fig. 5.1a and Fig. 5.1b. Upon immersion in water, the hydrophilic bars are expected to swell unlike the hydrophobic base, which is predicted to largely keep its initial dimension. By swelling, the triangular bars are supposed to expand in width and height as described in Fig. 5.3. It is assumed that the 3D object would consequently bend perpendicular to the extrusion axis of the hydrophilic bars, guided by the expansion of the upper part of the bars.

To confirm these hypotheses, the designed constructs were processed. The hydrophobic layer was printed first and then the hydrophilic part was added on top. To facilitate the detachment of the samples from the glass slide, the hydrophobic rectangular base part design includes an underlying array of pillars that could easily be cut with a scalpel blade

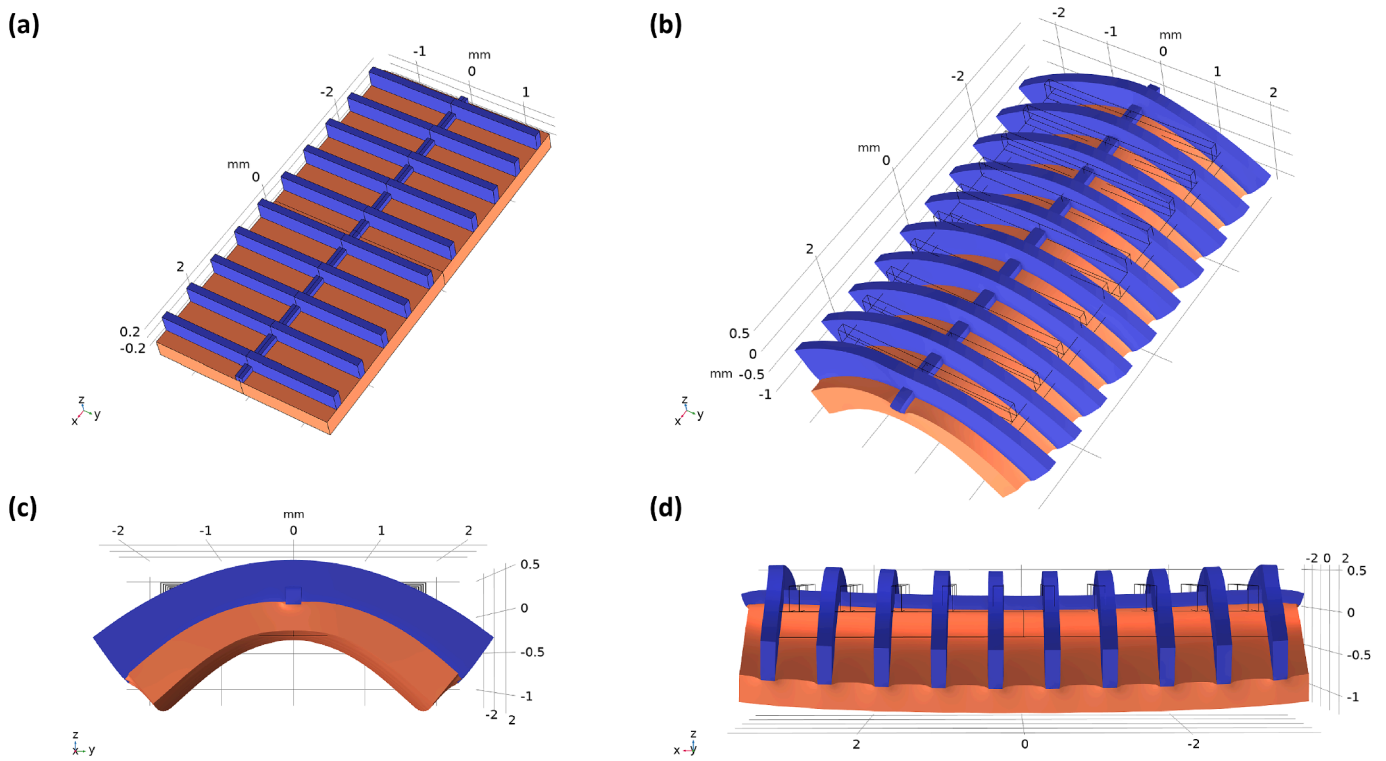

Fig. 6. Numerical modeling of a dual material 3D printable design predicted to only curl along one axis, with the hydrophobic and the hydrophilic materials shown in orange and blue, respectively. (a) Numerical modeling with the developed COMSOL model was iteratively employed to adjust the axial and perpendicular strains after swelling (b) to produce a fully swollen structure having (c) curl around the axial dimension, while remaining largely uncurled (d) along the perpendicular dimension. (For interpretation of the references to colour in this figure legend, the reader is referred to the web version of this article.)

(Supporting information, Figure S1). The resulting prints were post-treated by washing and drying, and the structure of the obtained materials was visually validated (Fig. 5.2). Finally, the samples were immersed in water. A rapid motion was observed upon immersion within the first minute, and then slowed down due to the slower swelling rate as shown by the swelling experiments (Fig. 3). This rapid actuation was reproduced by numerical modeling with most of actuation occurring within the first 60 s (Supporting information, Movie M2 and M3). Of notice, the conditions used to induce bending are compatible with physiological conditions as only hydration was required to trigger actuation. Visual inspection showed that swelling of the two printed objects resulted in largely equivalently bi-directional curled geometries after swelling (Fig. 5.4). Numerical modeling of the swelling process confirmed that a bi-directional curl is the mechanically least stressed configuration on swelling of both the printed dual-material geometry (Fig. 5.5). The bending of the prints parallel to the hydrophilic bars arises from the connected bars' isotropic expansion during swelling giving rise to a bi-axial stress at the interface between the materials. The temporal evolution of the object curling depends on the water transport rate into the materials. The numerical modeling shows that the majority of the shape change happens on minute time scale due to the small structural dimensions achievable by stereolithographic 3D printing (Supporting information, Movie M2 and M3).

Even if the 3D structure still needs to be optimized to control the motion precisely, this work demonstrated that methacrylate functional star-shaped PEG-PLA copolymers are good candidates for the development of sophisticated actuators using DLP. Indeed, dual materials could easily be printed and numerically predictable changes of shape could be observed when immersed in water. We explored predictive application of the developed COMSOL model to obtain a dual-material design that would selectively curl around a single axis as a simple example of engineering more complex topologies using layered 3D printing. The optimized 3D printable design is presented in Fig. 6a, with different views of the fully swollen design shown in Fig. 6(b-d). The cross-bar structures in the highly swellable hydrophilic material give rise to stress perpendicular to the axial dimension, while the lower stress induced by the axial bar structure of smaller cross-section provides axial rigidity without introducing axial curl. Interestingly, an equivalent geometry could not be attained during modeling if using an axial bar of equal height to the cross-bar structures, implying that high-resolution 3D printing does indeed provide unique opportunities to engineer complex swollen topologies.

Additionally, it is important to notice, that these actuators are composed of biomaterials that show a linear degradation in about 50 or 150 days depending on the hydrophilicity of the networks (Fig. S2a) and are cytocompatible according to ISO-10993 standard (Fig. S2b). In more details, under physiological mimicking conditions (phosphate saline buffer, pH 7.4, 37 °C) the more hydrophobic layer composed of crosslinked $PEG_{8arm}10k\text{-}(PLA_{69})_8$-MC due to its lower swelling showed a slow initial degradation with a mass loss limited to 15 % after 55 days followed by a faster and linear degradation phase to reach 95 % of degradation after 150 days. On the opposite, the more hydrophilic layer composed of crosslinked $PEG_{8arm}20k\text{-}(PLA_{13})_8$-MC showed a single and rapid linear degradation phase with 95 % of degradation at 55 days (Fig. S2a). The cytocompatibility towards L929 murine fibroblasts was confirmed following the extract method according to ISO-10993 with all layers showing a cell viability above the threshold of 70 % (Fig. S2b).

Taken together, this set of data confirm the ease of printing of these biomaterials, their facilitated combination thanks to their similar nature, their ability to yield hydration-based actuation systems as well as their degradability and cytocompatibility, which highlights their potential for the development of 4D-printed temporary medical devices.

4. Conclusion

This work highlights the great potential held by the family of star-

shaped PEG-PLA copolymers for 4D-printing of fully degradable swelling-based actuators from a single family of biocompatible degradable photopolymers. Both $PEG_{8arm}10k\text{-}(PLA_{69})_8$-MC and $PEG_{8arm}20k\text{-}(PLA_{13})_8$-MC could easily be 3D-printed with fast printing conditions to obtain crosslinked materials. Their high gel fractions and different water uptake confirmed their potential to be used for the design of water-responsive actuators. Thanks to their similar topology and chemical nature dual materials printing, which generally remains challenging by stereolithography, was easily reached via their formulation in resins of similar compositions that ensure comparable printing behaviors, as well as a cohesion of the polymeric networks at the interface. The design and printing of dual materials with complex shapes to develop water-responsive actuators was therefore made possible. This was illustrated with 3D-designs thought to produce hydrophobic/hydrophilic structures able to coil up in a controllable curled 3D shape on immersion in water. The designed 3D-shapes were successfully printed with a good resolution, and the observed deformation upon swelling could be modeled numerically. This set of results opens the door of resorbable and biocompatible biomaterials for 4D-printing and the development of degradable actuators based on hydration for biomedical applications *via* stereolithographic 3D printing.

CRediT authorship contribution statement

Mathilde Grosjean: Writing – original draft, Investigation. **Christina Schmidleithner:** Investigation. **Stéphane Dejean:** Investigation. **Niels B. Larsen:** Writing – original draft, Supervision, Conceptualization. **Benjamin Nottelet:** Writing – review & editing, Writing – original draft, Supervision, Funding acquisition, Conceptualization.

Declaration of competing interest

The authors declare that they have no known competing financial interests or personal relationships that could have appeared to influence the work reported in this paper.

Data availability

Data will be made available on request.

Acknowledgements

This work was supported by the ANR2019-OPENN (ANR-19-CE19-0022-02). The authors also thank the doctoral school “Sciences Chimiques Balard (ED 459)”, the “Fondation de la Maison de la Chimie” and the “Réseau des Ecoles Doctorales de Chimie Redox” for the international mobility grants. Authors thank the Synbio3 for access to the Size Exclusion Chromatography platform.

Appendix A. Supplementary data

Supplementary data to this article can be found online at https://doi.org/10.1016/j.matdes.2024.112953.

References

[1] L. Ionov, Polymeric actuators, Langmuir 31 (2015) 5015–5024, https://doi.org/10.1021/la503407z.
[2] P. Martins, D.M. Correia, V. Correia, S. Lanceros-Mendez, Polymer-based actuators: Back to the future, Phys. Chem. Chem. Phys. 22 (2020) 15163–15182, https://doi.org/10.1039/d0cp02436h.
[3] W. Li, Q. Guan, M. Li, E. Saiz, X. Hou, Nature-inspired strategies for the synthesis of hydrogel actuators and their applications, Prog. Polym. Sci. 140 (2023) 101665, https://doi.org/10.1016/j.progpolymsci.2023.101665.
[4] X. Wang, Y. He, Y. Liu, J. Leng, Advances in shape memory polymers: Remote actuation, multi-stimuli control, 4D printing and prospective applications, Mater. Sci. Eng. R Rep. 151 (2022) 100702, https://doi.org/10.1016/j.mser.2022.100702.
[5] M.A.C. Stuart, W.T.S. Huck, J. Genzer, M. Müller, C. Ober, M. Stamm, G. B. Sukhorukov, I. Szleifer, V.V. Tsukruk, M. Urban, F. Winnik, S. Zauscher, I. Luzinov, S. Minko, Emerging applications of stimuli-responsive polymer materials, Nat. Mater. 9 (2010) 101–113, https://doi.org/10.1038/nmat2614.
[6] G.I. Peterson, A.V. Dobrynin, M.L. Becker, Biodegradable shape memory polymers in medicine, Adv. Healthc. Mater. 6 (2017) 1700694, https://doi.org/10.1002/ADHM.201700694.
[7] C. Ohm, M. Brehmer, R. Zentel, Liquid crystalline elastomers as actuators and sensors, Adv. Mater. 22 (2010) 3366–3387, https://doi.org/10.1002/adma.200904059.
[8] I. Tokarev, S. Minko, Stimuli-responsive hydrogel thin films, Soft Matter. 5 (2009) 511–524, https://doi.org/10.1039/b813827c.
[9] M. Behl, K. Kratz, J. Zotzmann, U. Nöchel, A. Lendlein, Reversible bidirectional shape-memory polymers, Adv. Mater. 25 (2013) 4466–4469, https://doi.org/10.1002/adma.201300880.
[10] M. Behl, K. Kratz, U. Noechel, T. Sauter, A. Lendlein, Temperature-memory polymer actuators, Proc. Natl. Acad. Sci. USA 110 (2013) 12555–12559, https://doi.org/10.1073/pnas.1301895110.
[11] A. Zolfagharian, M. Denk, M. Bodaghi, A.Z. Kouzani, A. Kaynak, Topology-optimized 4D printing of a soft actuator, Acta Mech. Solida Sin. 33 (2020) 418–430, https://doi.org/10.1007/s10338-019-00137-z.
[12] A. Zolfagharian, A. Kaynak, A. Kouzani, Closed-loop 4D-printed soft robots, Mater. Des. 188 (2020) 108411, https://doi.org/10.1016/j.matdes.2019.108411.
[13] Z. Zhang, Y. Wang, Q. Wang, L. Shang, Smart film actuators for biomedical applications, Small 18 (2022) 2105116, https://doi.org/10.1002/smll.202105116.
[14] Q. Shi, H. Liu, D. Tang, Y. Li, X.J. Li, F. Xu, Bioactuators based on stimulus-responsive hydrogels and their emerging biomedical applications, NPG Asia Mater. 11 (2019) 1–21, https://doi.org/10.1038/s41427-019-0165-3.
[15] J.C. Breger, C. Yoon, R. Xiao, H.R. Kwag, M.O. Wang, J.P. Fisher, T.D. Nguyen, D. H. Gracias, Self-folding thermo-magnetically responsive soft microgrippers, ACS Appl. Mater. Interfaces. 7 (2015) 3398–3405, https://doi.org/10.1021/am508621s.
[16] Q. Jin, Y. Yang, J.A. Jackson, C. Yoon, D.H. Gracias, Untethered single cell grippers for active biopsy, Nano Lett. 20 (2020) 5383–5390, https://doi.org/10.1021/acs.nanolett.0c01729.
[17] E. Gultepe, J.S. Randhawa, S. Kadam, S. Yamanaka, F.M. Selaru, E.J. Shin, A. N. Kalloo, D.H. Gracias, Biopsy with thermally-responsive untethered microtools, Adv. Mater. 25 (2013) 514–519, https://doi.org/10.1002/adma.201203348.
[18] A. Ghosh, Y. Liu, D. Artemov, D.H. Gracias, Magnetic resonance guided navigation of untethered microgrippers, Adv. Healthc. Mater. 10 (2021) 2000869, https://doi.org/10.1002/adhm.202000869.
[19] K. Malachowski, M. Jamal, Q. Jin, B. Polat, C.J. Morris, D.H. Gracias, Self-folding single cell grippers, Nano Lett. 14 (2014) 4164–4170, https://doi.org/10.1021/nl500136a.
[20] Q. Zhao, J. Wang, H. Cui, H. Chen, Y. Wang, X. Du, Programmed shape-morphing scaffolds enabling facile 3D endothelialization, Adv. Funct. Mater. 28 (2018) 1801027, https://doi.org/10.1002/adfm.201801027.
[21] N. Bassik, B.T. Abebe, K.E. Laflin, D.H. Gracias, Photolithographically patterned smart hydrogel based bilayer actuators, Polymer (guildf) 51 (2010) 6093–6098, https://doi.org/10.1016/j.polymer.2010.10.035.
[22] K. Malachowski, J. Breger, H.R. Kwag, M.O. Wang, J.P. Fisher, F.M. Selaru, D. H. Gracias, Stimuli-responsive theragrippers for chemomechanical controlled release, Angew. Chem. - Int. Ed. 53 (2014) 8045–8049, https://doi.org/10.1002/anie.201311047.
[23] G. Stoychev, N. Puretskiy, L. Ionov, Self-folding all-polymer thermoresponsive microcapsules, Soft Matter. 7 (2011) 3277–3279, https://doi.org/10.1039/c1sm05109a.
[24] J.A. Luckanagul, C. Pitakchatwong, P. Ratnatilaka Na Bhuket, C. Muangnoi, P. Rojsitthisak, S. Chirachanchai, Q. Wang, P. Rojsitthisak, Chitosan-based polymer hybrids for thermo-responsive nanogel delivery of curcumin, Carbohydr. Polym. 181 (2018) 1119–1127, https://doi.org/10.1016/j.carbpol.2017.11.027.
[25] Y. Dai, P. Ma, Z. Cheng, X. Kang, X. Zhang, Z. Hou, C. Li, D. Yang, X. Zhai, J. Lin, Up-conversion cell imaging and ph-induced thermally controlled drug release from NaYF 4: Yb^{3+}/Er^{3+}@hydrogel core-shell hybrid microspheres, ACS Nano. 6 (2012) 3327–3338, https://doi.org/10.1021/nn300303q.
[26] X.Z. Zhang, P. Jo Lewis, C.C. Chu, Fabrication and characterization of a smart drug delivery system: Microsphere in hydrogel, Biomaterials 26 (2005) 3299–3309, https://doi.org/10.1016/j.biomaterials.2004.08.024.
[27] X.Z. Zhang, R.X. Zhuo, J.Z. Cui, J.T. Zhang, A novel thermo-responsive drug delivery system with positive controlled release, Int. J. Pharm. 235 (2002) 43–50, https://doi.org/10.1016/S0378-5173(01)00976-0.
[28] S. Kondaveeti, A.T.S. Semeano, D.R. Cornejo, H. Ulrich, D.F.S. Petri, Magnetic hydrogels for levodopa release and cell stimulation triggered by external magnetic field, Colloids Surfaces B Biointerfaces 167 (2018) 415–424, https://doi.org/10.1016/j.colsurfb.2018.04.040.
[29] L. Shang, W. Zhang, K. Xu, Y. Zhao, Bio-inspired intelligent structural color materials, Mater. Horizons. 6 (2019) 945–958, https://doi.org/10.1039/c9mh00101h.
[30] L. Sun, Y. Yu, Z. Chen, F. Bian, F. Ye, L. Sun, Y. Zhao, Biohybrid robotics with living cell actuation, Chem. Soc. Rev. 49 (2020) 4043–4069, https://doi.org/10.1039/d0cs00120a.
[31] J.U. Lind, T.A. Busbee, A.D. Valentine, F.S. Pasqualini, H. Yuan, M. Yadid, S. J. Park, A. Kotikian, A.P. Nesmith, P.H. Campbell, J.J. Vlassak, J.A. Lewis, K. K. Parker, Instrumented cardiac microphysiological devices via multimaterial three-dimensional printing, Nat. Mater. 16 (2017) 303–308, https://doi.org/10.1038/nmat4782.

[32] W. Zhao, C. Yue, L. Liu, Y. Liu, J. Leng, Research progress of shape memory polymer and 4D printing in biomedical application, Adv. Healthc. Mater. 12 (2023) 2201975, https://doi.org/10.1002/adhm.202201975.
[33] M. Afzali Naniz, M. Askari, A. Zolfagharian, M. Afzali Naniz, M. Bodaghi, 4D printing: A cutting-edge platform for biomedical applications, Biomed. Mater. 17 (2022) 062001, https://doi.org/10.1088/1748-605X/ac8e42.
[34] Y. Wang, H. Cui, T. Esworthy, D. Mei, Y. Wang, L.G. Zhang, Emerging 4D printing strategies for next-generation tissue regeneration and medical devices, Adv. Mater. 34 (2022) 2109198, https://doi.org/10.1002/adma.202109198.
[35] N. Paunović, D. Meyer, A. Krivitsky, A.R. Studart, Y. Bao, J.-C. Leroux, 4D printing of biodegradable elastomers with tailorable thermal response at physiological temperature, J. Control. Release 361 (2023) 417–426, https://doi.org/10.1016/j.jconrel.2023.07.053.
[36] X. Kuang, K. Chen, C.K. Dunn, J. Wu, V.C.F. Li, H.J. Qi, 3D printing of highly stretchable, shape-memory, and self-healing elastomer toward novel 4D printing, ACS Appl. Mater. Interfaces 10 (2018) 7381–7388, https://doi.org/10.1021/acsami.7b18265.
[37] B. Khatri, M. Frey, A. Raouf-Fahmy, M.V. Scharla, T. Hanemann, Development of a multi-material stereolithography 3D printing device, Micromachines 11 (2020) 532, https://doi.org/10.3390/mi11050532.
[38] Y. Wu, H. Su, M. Li, H. Xing, Digital light processing-based multi-material bioprinting: Processes, applications, and perspectives, J. Biomed. Mater. Res. - Part A. 111 (2022) 527–542, https://doi.org/10.1002/jbm.a.37473.
[39] M. Rafiee, R.D. Farahani, D. Therriault, Multi-material 3D and 4D printing: A survey, Adv. Sci. 7 (2020) 1902307, https://doi.org/10.1002/advs.201902307.
[40] C. Zhou, Y. Chen, Z. Yang, B. Khoshnevis, Digital material fabrication using mask-image-projection-based stereolithography, Rapid Prototyp. J. 19 (2013) 153–165, https://doi.org/10.1108/13552541311312148.
[41] K. Arcaute, B. Mann, R. Wicker, Stereolithography of spatially controlled multi-material bioactive poly(ethylene glycol) scaffolds, Acta Biomater. 6 (2010) 1047–1054, https://doi.org/10.1016/j.actbio.2009.08.017.
[42] G.I. Peterson, J.J. Schwartz, D. Zhang, B.M. Weiss, M.A. Ganter, D.W. Storti, A. J. Boydston, Production of materials with spatially-controlled cross-link density via vat photopolymerization, ACS Appl. Mater. Interfaces. 8 (2016) 29037–29043, https://doi.org/10.1021/acsami.6b09768.
[43] A. Muralidharan, A.C. Uzcategui, R.R. McLeod, S.J. Bryant, Stereolithographic 3D printing for deterministic control over integration in dual-material composites, Adv. Mater. Technol. 4 (2019) 1900592, https://doi.org/10.1002/admt.201900592.
[44] X. Kuang, J. Wu, K. Chen, Z. Zhao, Z. Ding, F. Hu, D. Fang, H.J. Qi, Grayscale digital light processing 3D printing for highly functionally graded materials, Sci. Adv. 5 (2019) eaav5790, https://doi.org/10.1126/sciadv.aav5790.
[45] W. Li, M. Bakhtiary Noodeh, N. Delpouve, J.M. Saiter, L. Tan, M. Negahban, Printing continuously graded interpenetrating polymer networks of acrylate/epoxy by manipulating cationic network formation during stereolithography, Express Polym. Lett. 10 (2016) 1003–1015, https://doi.org/10.3144/expresspolymlett.2016.93.
[46] C. Schmidleithner, R. Zhang, N. Taebnia, E.K.U. Larsen, K. Almdal, N.B. Larsen, High resolution dual material stereolithography for monolithic microdevices, Adv. Mater. Technol. 7 (2022) 2101180, https://doi.org/10.1002/admt.202101180.
[47] N.D. Dolinski, Z.A. Page, E.B. Callaway, F. Eisenreich, R.V. Garcia, R. Chavez, D. P. Bothman, S. Hecht, F.W. Zok, C.J. Hawker, Solution mask liquid lithography (SMaLL) for one-step, multimaterial 3D printing, Adv. Mater. 30 (2018) 1800364, https://doi.org/10.1002/adma.201800364.
[48] J.J. Schwartz, A.J. Boydston, Multimaterial actinic spatial control 3D and 4D printing, Nat. Commun. 10 (2019) 1–10, https://doi.org/10.1038/s41467-019-08639-7.
[49] D. You, G. Chen, C. Liu, X. Ye, S. Wang, M. Dong, M. Sun, J. He, X. Yu, G. Ye, Q. Li, J. Wu, J. Wu, Q. Zhao, T. Xie, M. Yu, H. Wang, 4D printing of multi-responsive membrane for accelerated in vivo bone healing via remote regulation of stem cell fate, Adv. Funct. Mater. 31 (2021) 2103920, https://doi.org/10.1002/adfm.202103920.
[50] J. Uribe-Gomez, A. Posada-Murcia, A. Shukla, M. Ergin, G. Constante, I. Apsite, D. Martin, M. Schwarzer, A. Caspari, A. Synytska, S. Salehi, L. Ionov, Shape-morphing fibrous hydrogel/elastomer bilayers fabricated by a combination of 3D printing and melt electrowriting for muscle tissue regeneration, ACS Appl. Bio Mater. 4 (2021) 1720–1730, https://doi.org/10.1021/acsabm.0c01495.
[51] Z. Song, L. Ren, C. Zhao, H. Liu, Z. Yu, Q. Liu, L. Ren, Biomimetic nonuniform, dual-stimuli self-morphing enabled by gradient four-dimensional printing, ACS Appl. Mater. Interfaces 12 (2020) 6351–6361, https://doi.org/10.1021/acsami.9b17577.
[52] M. Grosjean, S. Ouedraogo, S. Déjean, X. Garric, V. Luchnikov, A. Ponche, N. Mathieu, K. Anselme, B. Nottelet, Bioresorbable bilayered elastomer/hydrogel constructs with gradual interfaces for the fast actuation of self-rolling tubes, ACS Appl. Mater. Interfaces 14 (2022) 43719–43731, https://doi.org/10.1021/acsami.2c11264.
[53] R. Zhang, N.B. Larsen, Stereolithographic hydrogel printing of 3D culture chips with biofunctionalized complex 3D perfusion networks, Lab Chip. 17 (2017) 4273–4282, https://doi.org/10.1039/c7lc00926g.
[54] W. Hong, X. Zhao, J. Zhou, Z. Suo, A theory of coupled diffusion and large deformation in polymeric gels, J. Mech. Phys. Solids 56 (2008) 1779–1793, https://doi.org/10.1016/j.jmps.2007.11.010.
[55] W. Hong, Z. Liu, Z. Suo, Inhomogeneous swelling of a gel in equilibrium with a solvent and mechanical load, Int. J. Solids Struct. 46 (2009) 3282–3289, https://doi.org/10.1016/j.ijsolstr.2009.04.022.
[56] P.F. Jacobs, Fundamentals of stereolithography, Soc. Manuf. Eng. 196 (1992) 196–211.